# Narrow-azimuth migration: Analysis and tests in vertically layered media

*Biondo Biondi*[1]

**ABSTRACT**

Analysis of common-azimuth migration for vertically layered media shows that downward continuing the data in a narrow strip around the zero crossline offset should yield a kinematically correct migration scheme. I introduce two migration methods that exploit the common-azimuth equations to define an optimal range of crossline-offset wavenumbers and thus to minimize the number of crossline offsets that are necessary to sample adequately the crossline-offset dips. Tests on synthetic data generated assuming a vertically layered medium confirm the theoretical analysis and suggest further testing on data sets with complex velocity functions.

## INTRODUCTION

Common-azimuth is an attractive alternative to shot-profile migration for wave-equation 3-D prestack migration. It is computationally more tractable (Biondi and Palacharla, 1996) and it can easily generate Angle-Domain Common Image Gathers (ADCIG) (Prucha et al., 1999). In the past few years, we have shown that it produces good images both with challenging synthetic data (SEG/EAGE salt data set) (Biondi, 2000) and real data (Vaillant et al., 2000). However, in variable velocity, common-azimuth migration is not exact. In this paper, I generalize common-azimuth migration to overcome this limitation, following some of the ideas that we previously explored (Vaillant and Biondi, 1999, 2000). My aim is to define a method that is accurate in presence of arbitrary velocity variations.

I attack the problem by studying the simple case of vertically layered media, because the general case is difficult to analyze and numerical tests are expensive. On the contrary, in layered media, I can easily analyze the accuracy limitations of common-azimuth migration with the help of raytracing modeling and a synthetic data set modeled over five dipping planes.

I compare "raytracing migration" of an event with both the correct dispersion relation and its common-azimuth approximation. This analysis of the kinematics is consistent with the migration results of the synthetic data. It confirms previous results that even in the worst-case scenario for common-azimuth migration, (reflector's dip oriented at 45 degrees with respect to the acquisition geometry, and one reflections path close to overturn) the kinematics of

[1]**email:** biondo@sep.stanford.edu

common-azimuth migration are a good approximation of the kinematics of the exact migration.

The raytracing modeling also confirms that the departure of the exact raypaths from the common-azimuth assumption is small. For the particular example analyzed, the maximum crossline offset at depth is less than 200 m, when the full inline offset is 2.9 km. These results suggest that a narrow-azimuth extension to common-azimuth should be capable of handling correctly all the events in the data.

I thus define and test two narrow-azimuth schemes. Both schemes downward continue the data along a narrow crossline-offset strip, and take advantage of the common-azimuth equations to define the proper range of crossline-offset dips. The adaptation of the first schemes to lateral velocity variations is straightforward, and thus it is a good candidate for future tests on data with complex velocity. The second scheme is less affected by artifacts caused by the boundaries along the crossline-offset axis. It may have potential for fast and accurate migration when the velocity is only slowly varying as a function of the horizontal coordinates.

Tests on the synthetic data show that a narrow crossline-offset range (e.g. four or even two crossline offsets) is sufficient to obtain accurate migration results of the most steeply dipping (60 degrees) reflector in the synthetic data. These encouraging results suggest further test on more challenging data.

## ANALYSIS OF COMMON-AZIMUTH MIGRATION ERRORS

Kinematics of common-azimuth migration are only approximately correct when the velocity varies. The errors are related to the departure of the reflected events wavepaths from the common-azimuth geometry. This phenomenon can be easily understood by analyzing the raypaths of reflections. Figure 1 shows an example of raypaths for an event bouncing off a reflector dipping at 60 degrees and oriented at 45 degrees with respect to the offset direction. The offset is equal to 2.9 km, and the velocity function is $V(z) = 1.5 + .5z$ km/s. The projections of the rays on the crossline plane clearly show the raypaths departure from the common-azimuth geometry. Notice that the source ray (light gray) is close to overturn. A dipping reflector oriented at 45 degrees with rays close to overturn is the worst-case scenario for common-azimuth migration.

The event modeled with raytracing can also be imaged using raytracing by a simple process that I will identify as raytracing migration. Starting from the initial conditions at the surface given by modeling, both the shot and the receiver rays are traced downward until the sum of their traveltimes is equal to the traveltime of the reflected event. When raytracing migration is performed using the exact equation derived from an asymptotic approximation of the double-square root equation, the rays are exactly the same as the rays shown in Figure 1. On the contrary, if the common-azimuth approximation is introduced in the raytracing equations, the rays will follow the paths shown in Figure 2. As expected, the projections of the rays on the crossline plane overlap perfectly, confirming that the rays follow a common-azimuth geometry. However, in Figure 2 it is also apparent that the common-azimuth rays do not meet at the

ending points. This discrepancy in the kinematics causes errors in the migration. To connect the kinematic analysis with migration errors, I migrated a data set with similar characteristics as the events analyzed above. This data set was created by Louis Vaillant (Vaillant and Biondi, 2000). Data were generated using SEPlib `Kirmod3d` program. The reflectivity field consists of a set of five dipping planes, from zero dip to 60 degrees dip. The azimuth of the planes is 45 degrees with respect to the direction of the acquisition. The velocity was $V(z) = 1.5 + .5z$ km/s, which roughly corresponds to typical gradients found in the Gulf of Mexico. The maximum source-receiver offset was 3 km. Figure 3 shows the geometry of the reflectors.

Figure 4 shows a subset of the migration results. The front face of the cube displayed in the figure is an inline section through the stack. The other two faces are sections through the prestack image as a function of the offset ray parameter $p_{x_h}$. This migration results were obtained by including all the appropriate weighting factors, as discussed by Sava and Biondi (2001), including the phase shift and weights related to the stationary phase approximation.

Figure 5 shows an individual ADCIG gather from the same migrated image shown in Figure 4. The three events in the figure correspond to the planes dipping at 30, 45 and 60 degrees. Notice that the events are almost perfectly flat as a function of the offset ray parameter $p_{x_h}$, except for the reflections from the 60 degrees dipping plane with large offset ray parameters (i.e. large reflection angle). Figures 1- 2 show the rays corresponding to one of these events; in particular the one corresponding to $p_{x_h}$=.00045 s/m. Figure 6 shows the three orthogonal projections of these rays. The black (blue in colors) rays are the exact rays, while the light gray (cyan in colors) rays are the common-azimuth rays for the same events recorded at the surface. The solid (red in colors) dot corresponds to the imaging location for the common-azimuth migration. It is at the midpoint between the end points of the two rays. It is deeper than the correct one by $\Delta_z$=48 m, and laterally shifted by $\Delta_x$=-56 m and $\Delta_y$=-2 m. However, at fixed horizontal location, the dot is shallower by $\Delta_{\mathrm{z-plane}}$=-21 m than the reflecting plane. This is about the same vertical shift that is observable on the corresponding event in the ADCIG gather shown in Figure 5.

The maximum crossline offset of the exact rays is about 200 m. This maximum offset occurs at the intersection between the crossline offset ray parameter ($p_{y_h}$) curves shown on the top-right panel in Figure 6. This small value for the maximum crossline offset, compared with the inline offset, suggests the that event could be exactly downward continued by expanding the computational domain in a narrow strip around the zero crossline offset. However, to minimize the number of crossline offsets needed to adequately sample the crossline-offset dips ($p_{y_h}$), it is important to define an optimal range of $p_{y_h}$ that is not symmetric around the origin. In the next section I will discuss how to use the common-azimuth migration equations for defining such a range.

To evaluate the importance of not centering the range of $p_{y_h}$ at zero, I migrated the data assuming $p_{y_h} = 0$ for all events, and I also performed the corresponding raytracing migration. Figure 7 shows the same ADCIG gather as in Figure 5, but extracted from the image obtained assuming $p_{y_h} = 0$. In this gather the events are significantly frowning down. Furthermore, no image is present for the larger $p_{x_h}$. For example, the deeper reflector is not imaged at the ray parameter corresponding to the event represented in Figures 1- 2 ($p_{x_h}$=.00045 s/m). The lack

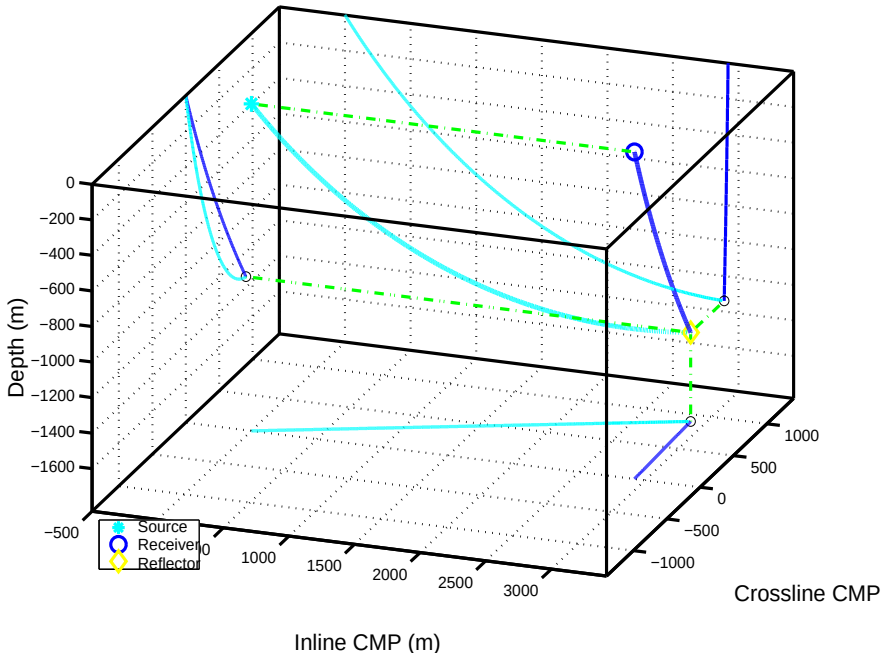


Figure 1: Ray corresponding to an event reflected by a reflector dipping at 60 degrees and oriented at 45 degrees with respect to the offset. The offset is 2.9 km offset, and $p_{x_h}$=.00045 s/m. The velocity function is $V(z) = 1.5 + .5z$ km/s. Notice the small, but finite, crossline offset of the rays at depth. Also notice that the source ray (light gray) is close to overturn. biondo1-sem1 [CR]

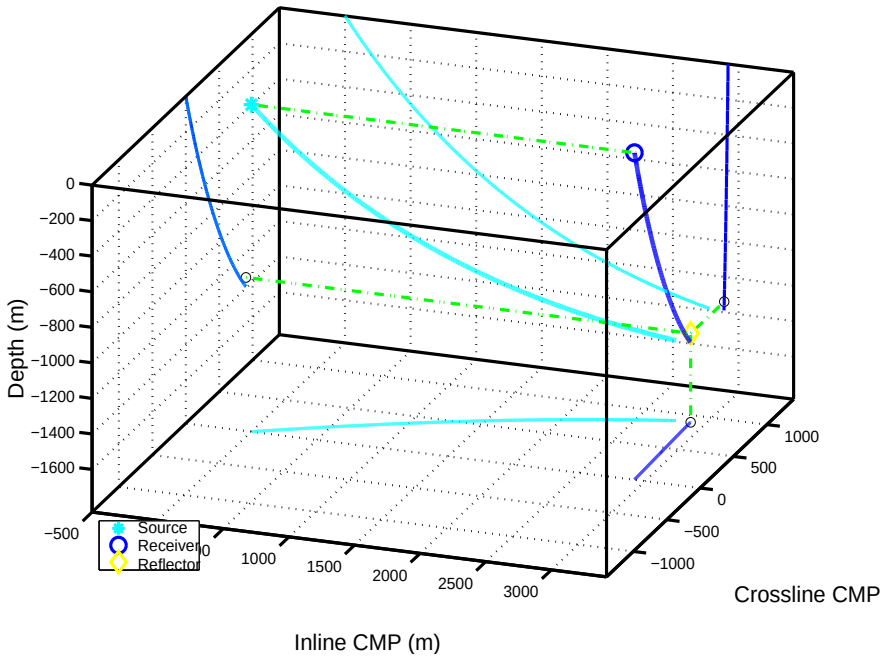


Figure 2: Equivalent common-azimuth rays for the same event shown in Figure 1. The common-azimuth rays are similar to the true rays shown in Figure 1, but the end points do not meet, causing a misspositioning of the migrated image. biondo1-sem2 [CR]

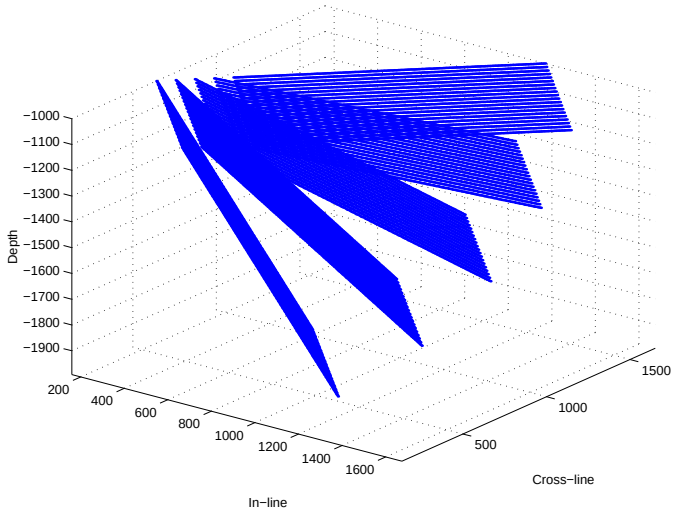


Figure 3: Geometry of the set of slanted planes, dipping at 0°, 15°, 30°, 45° and 60° towards increasing $x$ and $y$, at 45° with respect to the inline direction. biondo1-planes [NR]

of images is readily explained with raytracing. If the condition $p_{y_h} = 0$ is introduced in the raytracing equations one of the rays tends to overturn shallower than the true rays. Figure 8 shows the raytracing migration corresponding to $p_{x_h} = .000325 s/m$, one of the larger values of $p_{x_h}$ for which an event could be raytraced without neither of the rays overturning. The rays traced assuming $p_{y_h} = 0$ (light-gray lines) are clearly far from the correct rays (black lines). Figure 9 shows the corresponding common-azimuth raytracing migration for the same event ($p_{x_h} = .000325 s/m$) and offset 2.35 km. As for Figure 1, the solid dot corresponds to the imaging location for the common-azimuth migration. For common-azimuth migration the errors are much smaller than for $p_{y_h} = 0$, and about half than in Figure 6. The dot is deeper than the correct one by $\Delta_z$=22 m, and laterally shifted by $\Delta_x$=-23 m and $\Delta_y$=-4 m. At fixed horizontal location, the dot is shallower by $\Delta_{\text{z}-\text{plane}}$=-9 m than the reflecting plane. This is about the same vertical shift observable on the corresponding event in the ADCIG gather shown in Figure 5.

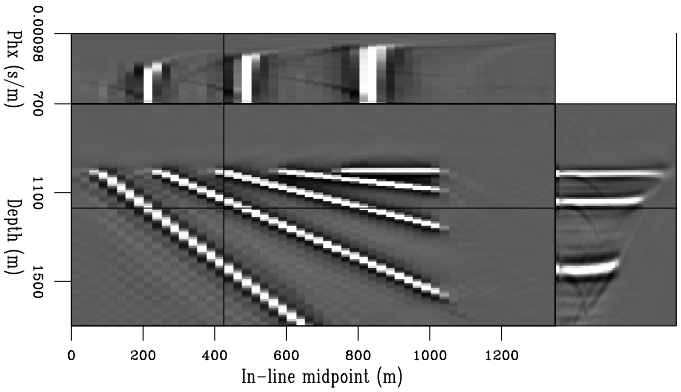


Figure 4: Subset of the results of common-azimuth migration of the synthetic data set. The front face of the cube is an inline section through the stack. The other two faces are sections through the prestack image. This migration results were obtained by including all the appropriate weighting factors, including the phase shift and weights related to the stationary phase approximation. biondo1-CA-pull-WKBJ-stat-vp [CR]

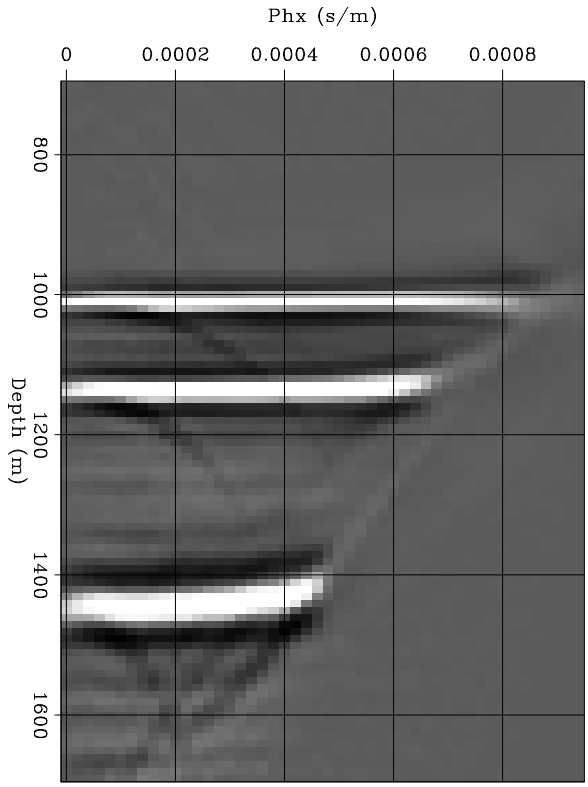


Figure 5: An ADCIG extracted from the same migrated image shown in Figure 4. The three events in the figure correspond to the planes dipping at 30, 45 and 60 degrees. Notice that the events are almost perfectly flat except for the large offset ray parameters (i.e. large reflection angle) of the 60 degrees dipping plane. biondo1-CIG-CA-pull-WKBJ-stat-cig [CR]

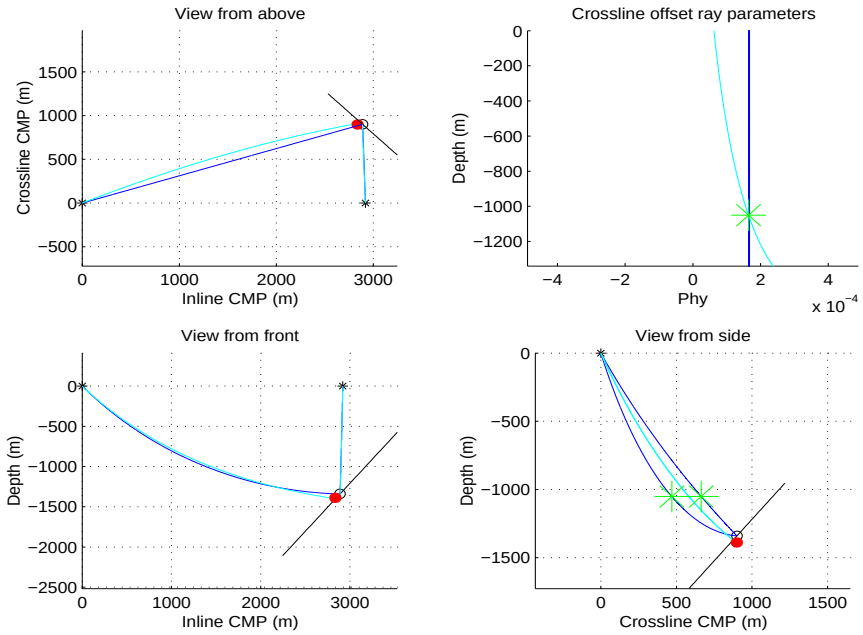


Figure 6: Orthogonal projections of rays shown in Figure 1 and Figure 2. The imaging point of common-azimuth migration (solid, red in colors, dot) is deeper than the correct one by $\Delta_z$=48 m, and laterally shifted by $\Delta_x$=-56 m and $\Delta_y$=-2 m. However, the dot is shallower by $\Delta_{z-\text{plane}}$=-21 m than the plane at the same horizontal location. This vertical shift is consistent with the shift observed in the ADCIG gather shown in Figure 5. The maximum cross-line offset of the exact rays is about 200 m. biondo1-sem3 [CR]

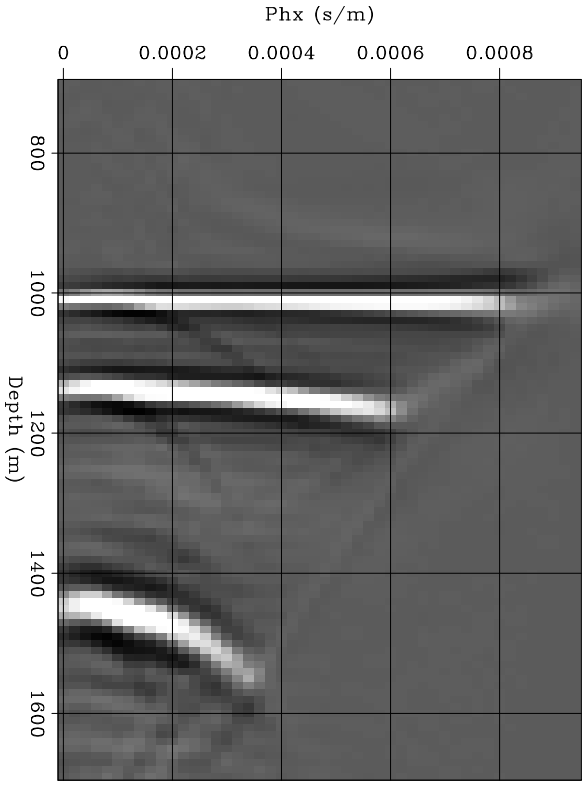


Figure 7: An ADCIG extracted from the migrated image obtained by assuming $p_{y_h} = 0$ during downward continuation. The three events in the figure correspond to the planes dipping at 30, 45 and 60 degrees. Notice that the events are frowning down and that no image is present at large ray parameters. biondo1-CIG-PS-1-nhy-WKBJ-stat-cig [CR]

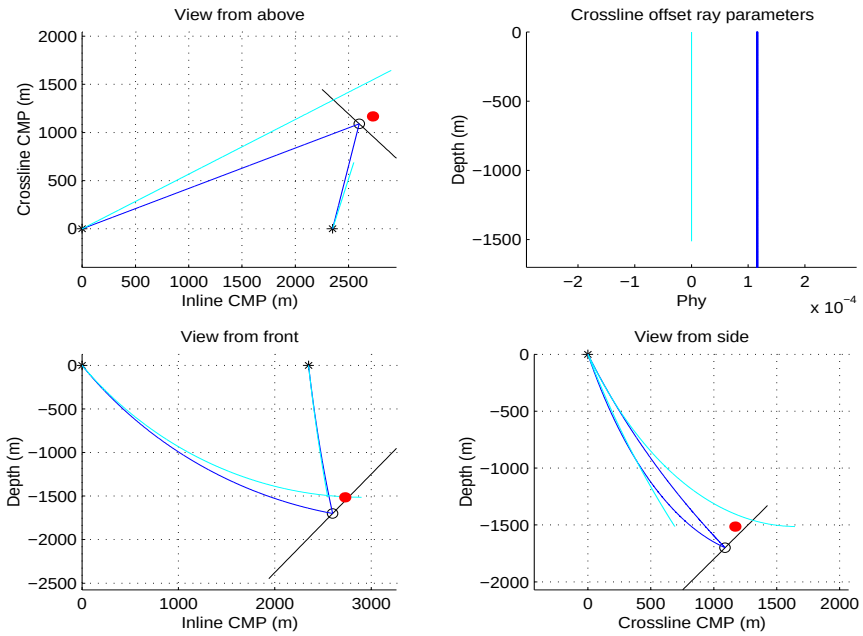


Figure 8: Orthogonal projections of rays tha are traced downward assuming $p_{y_h} = 0$ and corresponding to $p_{x_h}$=.000325 s/m and 2.35 km offset. biondo1-sem6 [CR]

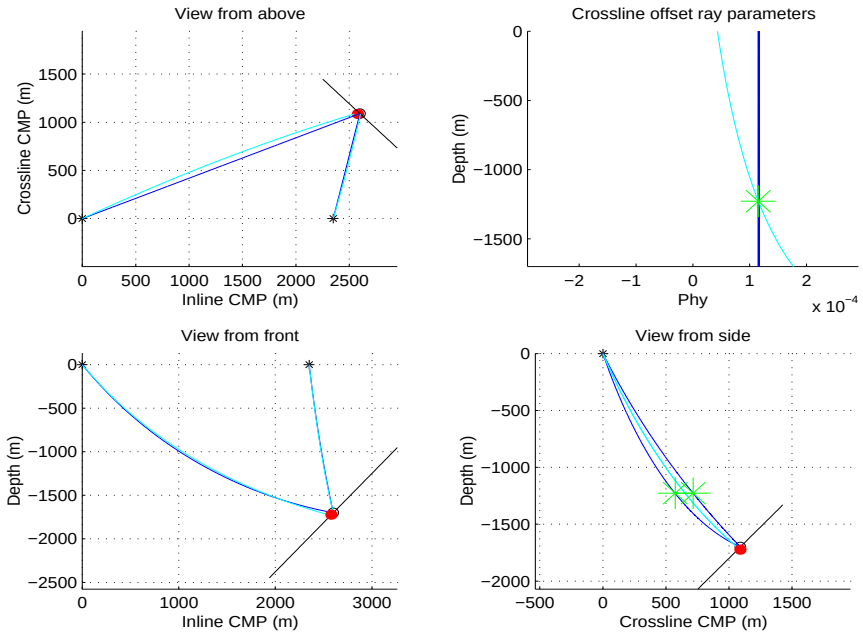


Figure 9: Orthogonal projections of rays for the same event as in Figure 8, but the rays are traced downward assuming common-azimuth geometry ($\Delta_z$=22 m, $\Delta_x$=-23 m, $\Delta_y$=-4 m, and $\Delta_{\text{z-plane}}$=-9 m). biondo1-sem5 [CR]

## TWO SCHEMES FOR NARROW-AZIMUTH MIGRATION

The kinematic analysis presented in the previous section suggests a generalization of common-azimuth migration based on the downward continuation of a narrow strip around the zero crossline offset. The computational cost of such a generalization is obviously proportional to the number of crossline offsets used to represent this narrow strip. The width of the strip is dependent on the reflector geometry and on the velocity model, but the sampling depends on the crossline-offset dip spectrum. To minimize the cost it is crucial to define an optimal criterion to define the range of crossline-offset dips ($p_{y_h}$). As demonstrated in the previous section, for dipping reflectors the dip spectrum is not centered around the zero dip ($p_{y_h} = 0$), and thus a symmetric range would be wasteful. I exploit the information provided by the common-azimuth equation to define a range of crossline-offset dips. For this reason I named my generalization narrow-azimuth migration, even if narrow crossline-offset would be a more accurate name.

The common-azimuth equation provides the crossline-offset dip $p_{y_h}$ as a function of the other dips in the data when the data are propagated along a constant azimuth (Biondi and Palacharla, 1996). In the frequency-wavenumber domain the common-azimuth relationship is:

$$\widehat{k_{y_h}} = k_{y_m} \frac{\sqrt{\frac{\omega^2}{v^2(\mathbf{g},z)} - \frac{1}{4}\left(k_{x_m} + k_{x_h}\right)^2} - \sqrt{\frac{\omega^2}{v^2(\mathbf{s},z)} - \frac{1}{4}\left(k_{x_m} - k_{x_h}\right)^2}}{\sqrt{\frac{\omega^2}{v^2(\mathbf{g},z)} - \frac{1}{4}\left(k_{x_m} + k_{x_h}\right)^2} + \sqrt{\frac{\omega^2}{v^2(\mathbf{s},z)} - \frac{1}{4}\left(k_{x_m} - k_{x_h}\right)^2}}. \tag{1}$$

where $\omega$ is the temporal frequency, $k_{x_m}$ and $k_{y_m}$ are the midpoint wavenumbers, $k_{x_h}$ and $k_{y_h}$ are the offset wavenumbers, and $v(\mathbf{s},z)$ and $v(\mathbf{s},z)$ are the local velocities. Ideally we would like to define a range of $k_{y_h}$ that is varying with depth, as a function of the local velocities. However, that may lead to complex implementation. For the moment I chose a simpler solution. I define a range of $k_{y_h}$ by setting a minimum velocity $v_{\min}$ and a maximum velocity $v_{\max}$, and define

$$k_{y_h}^{\min} = k_{y_m} \frac{\sqrt{\frac{\omega^2}{v_{\min}^2} - \frac{1}{4}\left(k_{x_m}+k_{x_h}\right)^2} - \sqrt{\frac{\omega^2}{v_{\min}^2} - \frac{1}{4}\left(k_{x_m}-k_{x_h}\right)^2}}{\sqrt{\frac{\omega^2}{v_{\min}^2} - \frac{1}{4}\left(k_{x_m}+k_{x_h}\right)^2} + \sqrt{\frac{\omega^2}{v_{\min}^2} - \frac{1}{4}\left(k_{x_m}-k_{x_h}\right)^2}}. \tag{2}$$

and

$$k_{y_h}^{\max} = k_{y_m} \frac{\sqrt{\frac{\omega^2}{v_{\max}^2} - \frac{1}{4}\left(k_{x_m}+k_{x_h}\right)^2} - \sqrt{\frac{\omega^2}{v_{\max}^2} - \frac{1}{4}\left(k_{x_m}-k_{x_h}\right)^2}}{\sqrt{\frac{\omega^2}{v_{\max}^2} - \frac{1}{4}\left(k_{x_m}+k_{x_h}\right)^2} + \sqrt{\frac{\omega^2}{v_{\max}^2} - \frac{1}{4}\left(k_{x_m}-k_{x_h}\right)^2}}. \tag{3}$$

The disadvantage of this solution is that the choice of $v_{\min}$ and $v_{\max}$ is somewhat arbitrary.

The central point of the $k_{y_h}$ range is then defined as a function of $k_{y_h}^{\min}$ and $k_{y_h}^{\max}$ as

$$\overline{k_{y_h}} = \frac{k_{y_h}^{\max} + k_{y_h}^{\min}}{2}, \tag{4}$$

and the range as

$$\overline{k_{y_h}} - \left(\frac{N_{y_h}}{2} - 1\right) dk_{y_h} \le k_{y_h} \le \overline{k_{y_h}} + \frac{N_{y_h}}{2} dk_{y_h}, \tag{5}$$

where $N_{y_h}$ is the number of crossline offsets and $dk_{y_h}$ is the sampling in $k_{y_h}$.

The two narrow azimuth schemes that I propose and tested differ in the definition of the crossline-offset wavenumber sampling $dk_{y_h}$. The first, and simplest, uses a constant value for $dk_{y_h}$; that is

$$dk_{y_h 1} = \frac{2\pi}{N_{y_h} \Delta y_h}. \tag{6}$$

The second one allows $dk_{y_h}$ to vary as

$$dk_{y_h 2} = \frac{k_{y_h}^{\max} - k_{y_h}^{\min}}{N_{y_h}}. \tag{7}$$

Varying $dk_{y_h}$ is equivalent to vary the width of the crossline-offset strip, and, at constant $N_{y_h}$, is also equivalent to vary the sampling $\Delta y_h$. At lower frequencies $dk_{y_h}$ is smaller, and thus the maximum crossline offset is larger. The migrated results benefit because the lower frequencies are the most affected by boundary artifacts and a wider strip reduces the artifacts caused by the boundaries. On the contrary, as the frequency increases, $dk_{y_h}$ is larger and $\Delta y_h$ smaller, and thus spatial aliasing is avoided.

The main disadvantage of this second scheme is that the transformation between space and wavenumber domains becomes more cumbersome. Mixed space/wavenumber domain downward-continuation methods (Biondi, 1999) become more expensive, and thus the scheme becomes less attractive when the velocity is laterally varying.

**Migration tests**

I run both narrow-azimuth migration methods on the synthetic data set described above, varying the number of crossline-offset samples $N_{y_h}$ from 2 to 16. To create data with more than one crossline offset I padded the common-azimuth data with zeros. I also run a full phase-shift 3-D prestack migration on the same data. Full phase-shift 3-D prestack migration is equivalent to the first method of narrow-azimuth migration, but with the $k_{y_h}$ range centered at $k_{y_h} = 0$, instead of at the $\overline{k_{y_h}}$ given by equation (4).

For both the full phase-shift migration and the first narrow-azimuth methods, I kept the maximum value of the crossline offset constant at 800 m for all values of $N_{y_h}$. Therefore, according to equations (6) and (5) the sampling rate of $k_{y_h}$ was independent of $N_{y_h}$, but the range of $k_{y_h}$ decreased as $N_{y_h}$ decreased. Both methods lose accuracy as the range of $k_{y_h}$ decreases, but the accuracy of full phase-shift migration degrades quicker than the accuracy of narrow-azimuth migration.

For all of these tests I used all the appropriate weighting factors, as discussed by Sava and Biondi (2001), except the phase shift and weights related to the stationary phase approximation. I excluded the stationary phase correction because as the range of $k_{y_h}$ increases it is not anymore necessary. Indeed, the phase of the migrated images changes as the $N_{y_h}$ increases. However, the amplitude of the deeper reflectors decreases as $N_{y_h}$ increases because of the increasing amount of zero padding.

Figure 10 shows the the results of full phase-shift migration of the synthetic data set with $N_{y_h} = 16$. It shows the same subset of the migrated cube as in Figure 4. The front face of the cube is an inline section through the stack. The other two faces are sections through the prestack image. The kinematics of the migration are correct. The events are flat in the ADCIG shown in Figure 11. I use this results as benchmark for the narrow-azimuth and the full phase-shift migration as $N_{y_h}$ decreases.

Figures 12 shows two ADCIGs, taken at the same location as the ADCIG in Figure 11, but obtained with $N_{y_h} = 8$. The ADCIG on the left (a) was obtained by full phase-shift migration, and the ADCIG on the left (a) was obtained by the first method for narrow-azimuth migration. For narrow azimuth-migration I used $v_{\min} = 1.8$ km/s and $v_{\max} = 2.1$ km/s. The kinematics of the narrow-azimuth migration are correct. On the contrary, the results of full phase shift migration begin to degrade at larger $p_{x_h}$.

Figures 13 and 14 shows the same ADCIGs as in Figure 12, but with respectively $N_{y_h} = 4$ and $N_{y_h} = 2$. The kinematics of the narrow-azimuth migration are correct for $N_{y_h} = 4$ and show only a slight degradation at large $p_{x_h}$ for $N_{y_h} = 2$. On the contrary, the results of full phase shift migration are poor even at small $p_{x_h}$.

Finally, I compare the results of using the two methods for narrow-azimuth migrations that I presented in the previous section. Figure 15 shows the ADCIGs taken at the same location as in Figure 12, also obtained with $N_{y_h} = 8$. The ADCIG on the left is obtained using the second narrow-azimuth method; that is, when using equation (7) to determine the sampling rate for $k_{y_h}$. The ADCIG on the right is obtained using the first narrow-azimuth method; that is, when

using equation (6) to determine the sampling rate for $k_{y_h}$. The kinematics of the two images are equivalent. However, the image obtained using the second method has less artifacts caused by the boundaries along the crossline-offset axis.

## CONCLUSIONS

In vertically layered media, reflected events have a limited crossline offset at depth even in the worst-case scenario for common-azimuth geometry. This result confirms the robustness of common-azimuth migration and leads to its generalization obtained by downward continuing the data in a narrow strip around the zero crossline offset. Both narrow-azimuth migration methods that I propose in this paper achieve high efficiency by exploiting the common-azimuth equations to define an optimal range of crossline-offset wavenumbers.

Tests on synthetic data generated assuming a vertically layered medium show that very few (2 or 4) crossline offsets are needed to obtain migrated images with the correct kinematics.

## REFERENCES

Biondi, B., and Palacharla, G., 1996, 3-D prestack migration of common-azimuth data: Geophysics, **61**, no. 6, 1822–1832.

Biondi, B. L., 1999, 3-D Seismic Imaging: `http://sepwww.stanford.edu/sep/biondo/Lectures/index.html`.

Biondi, B., 2000, 3-D wave-equation prestack imaging under salt: 70th Ann. Internat. Mtg., Soc. Expl. Geophys., Expanded Abstracts, 906–909.

Prucha, M., Biondi, B., and Symes, W., 1999, Angle-domain common-image gathers by wave-equation migration: 69th Ann. Internat. Meeting, Soc. Expl. Geophys., Expanded Abstracts, 824–827.

Sava, P., and Biondi, B., 2001, Amplitude-preserved wave-equation migration: SEP–**108**, 1–26.

Vaillant, L., and Biondi, B., 1999, Extending common-azimuth migration: SEP–**100**, 125–134.

Vaillant, L., and Biondi, B., 2000, Accuracy of common-azimuth migration approximations: SEP–**103**, 157–168.

Vaillant, L., Calandra, H., Sava, P., and Biondi, B., 2000, 3-D wave-equation imaging of a North Sea dataset: Common-azimuth migration + residual migration: 70th Ann. Internat. Mtg., Soc. Expl. Geophys., Expanded Abstracts, 874–877.

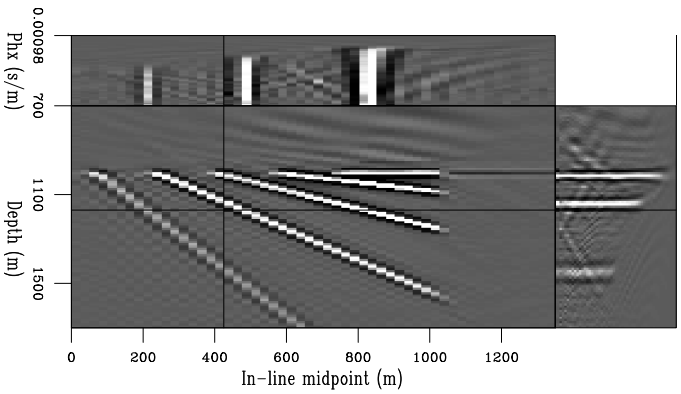


Figure 10: Subset of the results of full phase-shift migration of the synthetic data set with $N_{yh} = 16$. The front face of the cube is an inline section through the stack. The other two faces are sections through the prestack image. biondo1-PS-16-nhy-WKBJ-vp [CR]

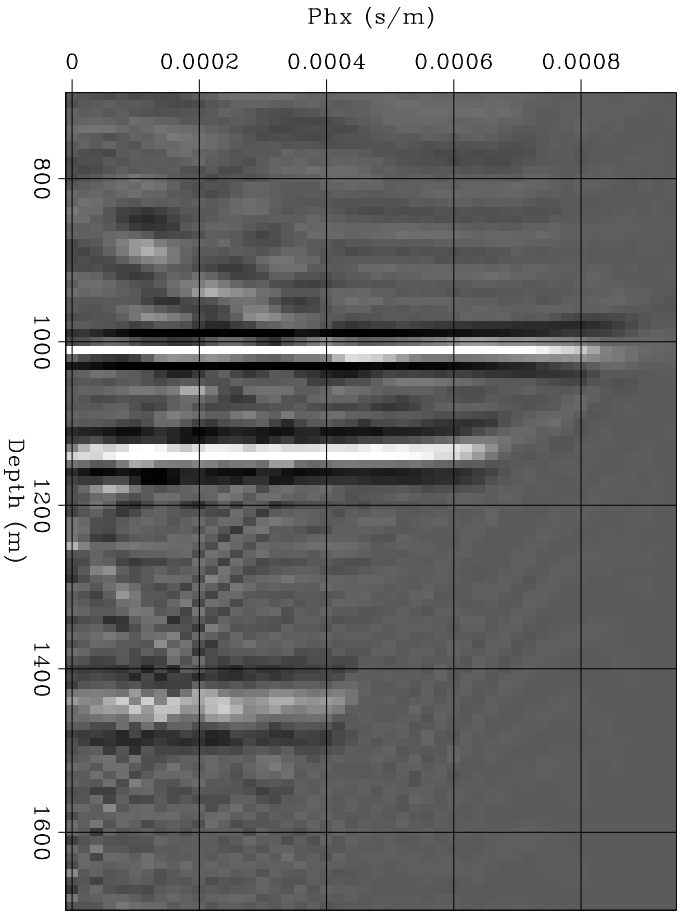


Figure 11: An ADCIG extracted from the same migrated image shown in Figure 10. The three events in the figure correspond to the planes dipping at 30, 45 and 60 degrees. Notice that the events are perfectly flat. biondo1-CIG-PS-16-nhy-WKBJ-cig [CR]

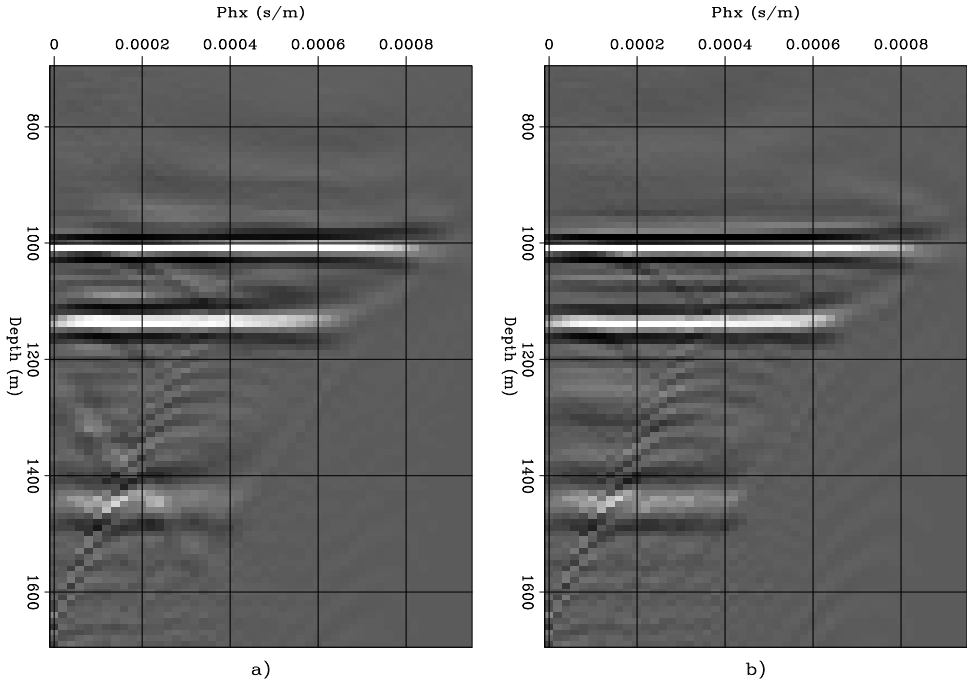


Figure 12: ADCIGs extracted from the migrated image obtained with $N_{y_h} = 8$ for a) full-phase shift migration, and b) narrow-azimuth migration. biondo1-CIG-both-8 [CR]

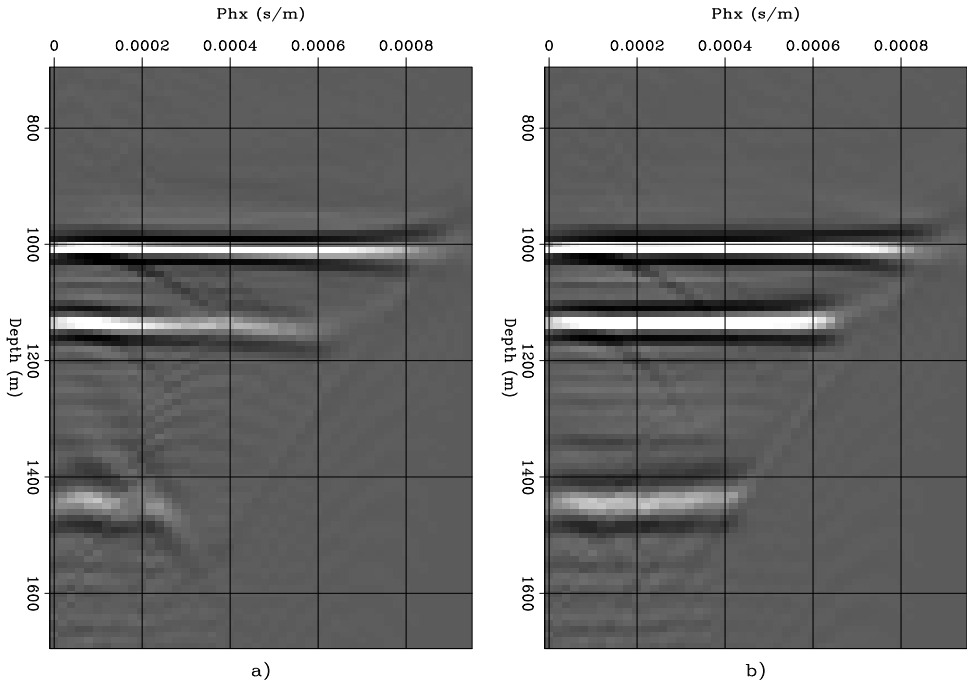


Figure 13: ADCIGs extracted from the migrated image obtained with $N_{y_h} = 4$ for a) full-phase shift migration, and b) narrow-azimuth migration. biondo1-CIG-both-4 [CR]

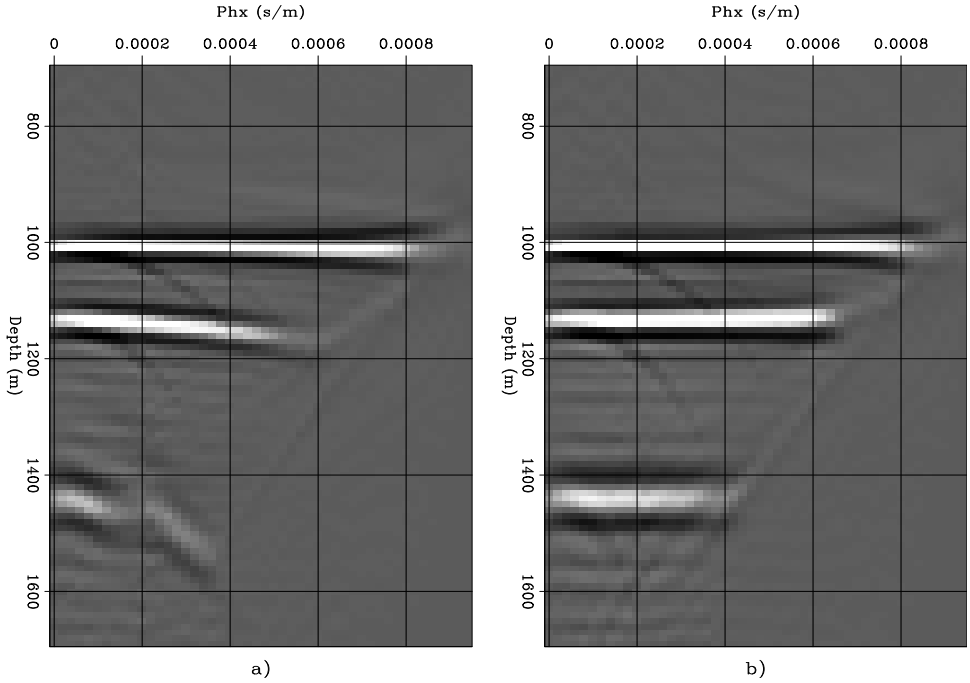


Figure 14: ADCIGs extracted from the migrated image obtained with $N_{y_h} = 2$ for a) full-phase shift migration, and b) narrow-azimuth migration. biondo1-CIG-both-2 [CR]

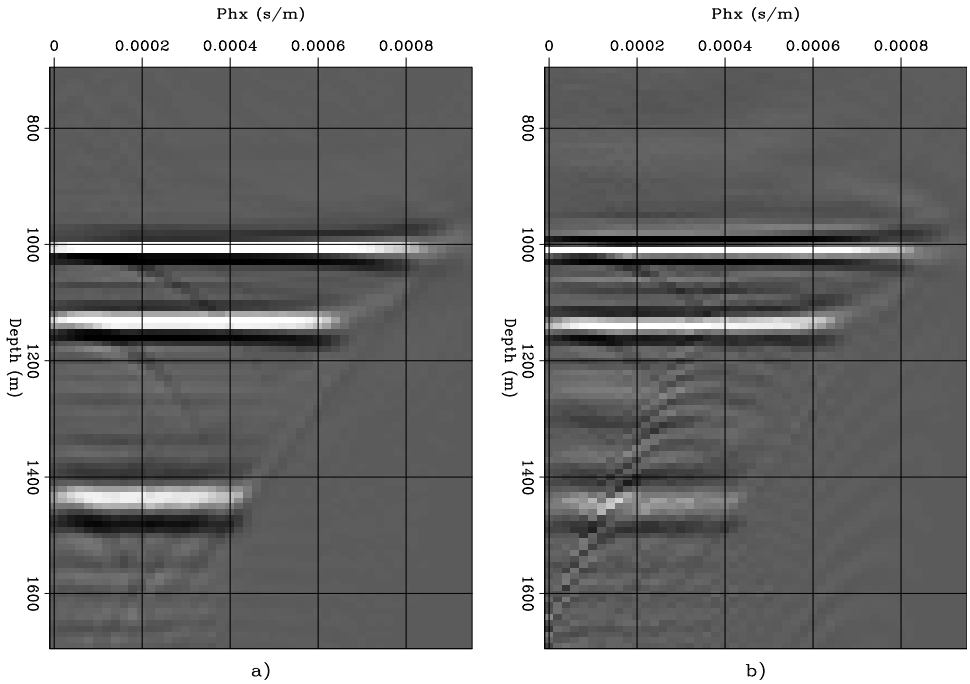


Figure 15: ADCIGs extracted from the migrated image obtained with $N_{y_h} = 8$ for a) narrow-azimuth migration with $dk_{y_h}$ from equation (7), and b) narrow-azimuth migration with $dk_{y_h}$ from equation (6). biondo1-CIG-8-uneven [CR]